Effects of surface topography at different scales on the dispersion of the wetting data for sessile water droplets on nitrided austenitic stainless steels

Thierry Czerwiec, Svetlana Tsareva, Aurore Andrieux, S. Bruyere, Grégory Marcos

Version of Record: https://www.sciencedirect.com/science/article/pii/S0257897222004315
Manuscript_181c4892c67b883fc7e955097f5def9d

Effects of surface topography at different scales on the dispersion of the wetting data for sessile water droplets on nitrided austenitic stainless steels

T. Czerwiec[a,b], S. Tsareva [a], A. Andrieux [a], S. Bruyère[a], G. Marcos [a,b]

[a] *Institut Jean Lamour (IJL), Département CP2S, UMR 7198 CNRS, Université de Lorraine, 2 allée André Guinier, BP 50840, 54000 Nancy, France..*
[b]*Laboratoire d'Excellence Design of Alloy Metals for low-mAss Structures (LabEx DAMAS), Université de Lorraine, Ile du Saulcy, F-57045 Metz cedex, France*

* thierry.czerwiec@univ-lorraine.fr, phone + 33 3 72 74 24 98

ABSTRACT

Plasma nitriding is used to increase the durability of steels. The wettability of nitrided surfaces is poorly studied. The ability of nitriding in modifying the wetting and evaporation of sessile droplets on austenitic stainless steel is studied. Transferred plasma for nitriding provides independent substrate biasing giving the opportunity to tailor the surface before and during the nitriding treatments. It was shown that a cleaning treatment (Ar-H_2 plasma) produces topographical modifications of the surface by selective sputtering of the grains giving contact angles between 80 and 90 °. Similar results are obtained when the nitriding treatments are carried out with a rather high bias voltage. It is explained using the skewness (Ssk) topographical roughness parameter which reveals the asymmetry of the profile. The more the Ssk is, the higher the contact angle is. During nitriding treatments, the very high internal stresses leads to the formation of spikes at the grain boundaries. Pinning of the three-phase contact line on peaks localized at grain boundaries are responsible for high contact angles. For nitriding treatments carried out with lower bias, surface contamination occurs and a discontinuous oxynitride layer is formed. The nanostructure formed by these oxides gives contact angles up to 120 °.

Keywords

wettability, surface topography, nitriding, water droplets,

1. Introduction

Wetting and evaporation of sessile droplets on a solid surface is interesting both from the fundamental and from the industrial point of view [1-3]. Evaporation on engineered surfaces is now intensively studied, especially on those having superhydrophobic properties [4] inducing self-cleaning, low adhesion surfaces, drag reduction for fluid flows [5], anti-icing (icephobic) [6], anti-fogging, anti-fouling, water/oil separation, fluid transport [7], biological microarrays [8], friction reduction [9], anti-corrosion [10], energy [11-12]. Improving phase change heat transfer is important to meet the rising global energy demand in a sustainable manner in various industrial applications: thermal generation of electricity, desalination, metallurgy, electronics cooling, heat exchangers and food processing [13].
Variations in geometrical parameters (contact angle and radius) over time of a droplet placed on a functionalized surface are a simple experimental way to study wetting and evaporation. Although the geometry of a sessile droplet is relatively simple, it is representative of real-life situations (for example, metallic inks for inkjet printing, the spreading of pesticides on leaves, the spreading of blood serum, etc..) [14]. However, the understanding of wetting and

evaporation of a simple droplet is non-trivial due to the full coupling with the substrate upon which the drop is deposited, the atmosphere surrounding the droplet, and the nature of the fluid [15-16]. Surface functionalization leading to contrasted physical properties, patterning, hierarchical or decoupled hierarchical structures is an active subject of research [11-13,17-18]. The durability of these functionalized surfaces is a major issue for their large-scale use [16-23]. Plasma nitriding is widely used to improve the surface properties of steels and is an attractive way to increase the durability of steel surfaces processed for wetting and evaporation performances [24]. During nitriding treatments of steels, species containing nitrogen in activated form (atomic nitrogen, excited nitrogen molecules, NH_x radicals,…) are adsorbed on the surfaces and atomic nitrogen can then be absorbed in the bulk of steels [25-26]. These stages, which are still relatively unknown, are very sensitive to the state of the extreme surface as is the wettability. Depending on the steel, solid solution of nitrogen in steel or some nitrides (oxynitrides) can be formed after these initial stages. Before starting a plasma assisted nitriding (PAN) treatment, a plasma cleaning step is generally carried out in order to remove superficial oxide films that can be found at the steel surface, especially for stainless steels that forms passive layers. This surface activation has a great influence on both the nitrided layers thickness and composition [27-31]. PAN treatments are mostly performed using pulsed DC discharges at moderate pressure (100-1000 Pa), for which -most of the time- the plasma reactivity is coupled to the substrate heating. In these conventional PAN treatments, it is the bias voltage that allows the adjustment of the substrate temperature, which is a crucial parameter in nitriding. However, changing the bias voltage also modify the ion bombardment and thus the sputtering of the substrate during a PAN treatment [30-31]. More flexibility and control are provided by the so-called “transferred plasma” concept [25]. A common feature of these high density sources is the uncoupling of the plasma generation from the substrate surface. In such processes, independent substrate biasing provides a means for independent ion flux and ion energy control. Such advantages are also available during the cleaning step before a PAN treatment. A review of the different plasma processes and the different gas mixtures used during a cleaning step before PAN treatment of austenitic stainless steel can be found in [30]. Strangely, the wettability of nitrided surfaces is poorly studied in the literature [30]. The purpose of this communication is to study the ability of nitriding treatments in modifying the wetting and evaporation of sessile droplets on AISI 316L. A careful attention is given to both the effect of the plasma cleaning step and on the role of the ion bombardment during a nitriding treatment.

We will first present a literature review on the wettability of nitrided austenitic stainless steel surfaces as well as preliminary results which motivated this study. The evolution of the geometric parameters of the drops (contact angle and radius) as a function of time for nitriding conditions in which the bias voltage has been modified will be described and commented. Observations carried out by optical and confocal microscopy as well as by SEM and by TEM will allow us to propose explanations on the differences of contact angles measured on the nitrided surfaces. In this paper, evaporation data are presented for the first on nitrided austenitic stainless steel. These data will be discussed using existing theories. It will be also shown that these theories explain well most of the data presented in this paper. This is connected to the topography at the micrometric scale and the pinning of the three-phase contact line on peaks localized at grain boundaries. However, it these theories fails to explain some of our experimental data obtained on nitrided samples on which a layer of nanometric oxynitrides particles is present. It will be also shown that the presence of these particles can be modified by ion bombardment.

2. Experimental

The samples used in this communication are tempered AISI 316L stainless steel cylinders rod (20 mm of diameter, thickness of less than 5 mm) with different composition (table 1). The sample are prepared by mechanical polishing until mirror-like surface state (SiC emery paper to 4000 grit (5 µm) followed by polishing with 3 µm et 1 µm diamond paste), cleaned with ethanol, distilled water and dried by compressed air. A multi-dipolar electron cyclotron resonance system (MDECR) was used for the nitriding experiments. A more complete description of the reactor can be found in [32-33].

Samples	**Fe**	**Cr**	**Ni**	**Mn**	**Mo**	**Si**	**Cu**	**Co**	**N**	**P**	**C**	**S**	**O**
1	Comp.	16.7	10.1	1.5	2.1	0.03	0.5	0.2	0.05	0.03	0.02	0.03	n.m.
2	Comp.	16.2	9.4	2.6	2	0.9	0.7	0.2	0.10	0.05	0.02	0.02	0.3
3	Comp.	16.4	9.4	2.3	2	0.9	0.7	0.2	0.09	0.05	0.02	0.02	0.3
M	Comp.	16.7	13.9	2.6	2.6	0.7	0.4	0.1	0.07	0.04	0.02	0.00	0.2

Table 1. Composition of the different AISI 316L stainless steel samples in wt%.

Hydrogen is provided by an hydrogen gas generator (NM-H2 500 from F-DGSi). The experimental conditions are described in table 2. Before the nitriding treatment, an in-situ cleaning pre-treatment, intended to remove the native oxide layer, was performed in 50% Ar-50% H_2 at a pressure of 2 Pa for 30 min, with an incident microwave power of 600 W and a bias voltage of – 100 V. The plasma was maintained in between this first step and the nitriding step to reach the treatment temperature. Additional heating of the substrate is provided by an heating system integrated to the substrate holder. The temperature of the samples was measured with a thermocouple embedded in a substrate.

Sample preparation	Type of pre-treatment	Type of treatment	Bias during the plasma treatment	Type of sample and **sample name**	Initial contact angle θ_i (°)	Related figures	Evaporation time t_f (s)
Polished	no	no	/	1 (set 1)	60	1	/
Polished	Ar-50% H_2 bias -100 V 2 Pa, 600 W for 30 min	90% N_2-10% H_2 2 Pa, 600 W at 400°C	- 50	1 (set 1)	62 to 108.5	1	/
Polished	50% Ar-50% H_2 bias -100 V 2 Pa, 600 W for 30 min	90% N_2-10% H_2 2 Pa, 600 W at 400°C	- 50	1 (set 2) After nitriding followed by 2 polishing steps	88 to 35	1	/
Polished	/	/	/	2, 3, M time after polishing (0,3,7,10 days) **polished time evolution**	42 to 63	4, 11	556 to 860
Polished	/	50% Ar-50% H_2 2 Pa, 600 W for 2 h	- 100	2, 3, M Several days after the treatment **(sputtered 2 h)**	82.4 to 94.1	4, 11	519 to 684
Polished	/	95% Ar-5% H_2 2 Pa, 600 W for 8 h	- 400	M Several days after the treatment **(sputtered 8 h)**	74.4	4, 11	928
Polished	squares of 100 × 100 µm separated by 200 µm from each other with a depth of 0.7 µm prepared by sputtering in Ar-H_2 plasma [42]			1 **patterned**	85.8	4, 11	1100
Polished	Ar-50% H_2, bias -100 V 2 Pa, 600 W for 30 min	90% N_2-10% H_2 2 Pa, 600 W at 400°C	Mostly - 50 0 and -100	2, 3, M **nitrided**	78.4 to 118.2	4, 11	305 to 1164

Table 2. Samples preparation, treatments parameters and data related to wetting

The analysis of the drop traces on the samples was performed by optical microscopy. Contact angle measurements were performed with a Digidrop equipment at room temperature (22-23°C) with a air humidity of 50%. Drops of bidistilled water (conductivity 55 $\mu\Omega.m^{-1}$) were deposited with minimal influence of external forces and the process was recorded until the drop was fully evaporated, with 1 picture taken per second. The droplet volume was 1 µl unless specified in the text and each measure was repeated 5 times. Before measurements, the samples were cleaned using ethanol, acetone and distilled water, and dried.

Profiles of the treated surfaces were measured using a white light interferometer (smartWLI extended GBS-Ilmenau GmbH) with a × 50 magnification (lateral resolution 0.66 µm). Data analysis were performed using the Mountains Map© software. For the preliminary results presented in part 3, a simple procedure based on profile analysis was applied. A more robust procedure was applied to the other measurements. The procedure used meets the ISO 25178 standard for which we have applied a robust Gaussian filter to separate undulation and roughness profiles. The sampling area was 155*215 μm^2 and the measurements were repeated 2 times.

The analysis of the microstructure of the nitrided samples was performed by scanning electron microscopy (SEM, EI Quanta-FEG-650 - EDS QUANTAX Bruker) and optical microscopy. Local surface topography of samples was studied by using an AFM equipment from CSInstruments (model Nano Observer) in the contact mode.

Cross-section foils were prepared using a scanning electron microscope (Helios Nanolab 600i) associated with a source of focused ions (FIB). Two platinum layers were deposited to protect the surface of the sample during the preparation phase. A JEOL ARM 200F microscope equipped with a cold field emission gun, a high resolution lens as well as a EDS detector (energy dispersive X-ray spectroscopy) JEOL Centurio was used for TEM measurements. This microscope operating at 200 kV notably allowed observation in high TEM mode resolution (HRTEM - with a parallel electron beam and point-to-point resolution: 0.19 nm) of nanostructures present in FIB foils. The scanning mode (STEM - the electron beam is convergent and a spatial resolution of 0.08 nm) coupled to the EDS detector was used to recording of elementary maps. The so-called (high angle annular dark field) detector collects the electrons scattered in an almost inelastic way located farthest from the optical axis of the microscope. Theses STEM-HAADF images are sensitive to elementary composition.

3. Background on wetting of nitrided surfaces and preliminary experiments

A recent very good review was done by Borgioli on the wetting of nitrided stainless steel by water [30]. There are very few publications and the changes of wetting behavior were investigated mainly for biocompatibility. We will limit our interest to the papers related to AISI 316L, except for references [31-34] in which AISI 202 was used. The obtained results are not indicating a clear tendency for the nitrided surfaces. For some researchers, the contact angle (CA) of water drops on nitrided specimens is reported to decrease [33-37] or to increase [30-33, 39-41], in comparison with that for untreated samples. For Lin et al. [35] the CA is found to decrease with the nitriding treatment time (from 40 to 80 min. at 450°C). Buhagiar et al. [36] reported very low CAs (40 to 50°). Galeano-Osorio et al. [37] have observed an increase for the CAs as the nitriding temperature is increased from 380 to 420°C for treatments of 2 h (the contact angle for the samples nitrided at 420 °C became comparable to that of the untreated ones 94.5°, drop volume of 2.5 µl). Braz et al. [38] measured a CA of 72° (drop volume of 20 µl) for a sample nitrided 1h at 450°C as compared to a CA of 100° for the untreated sample. One common point to these research is the high CA of the non-treated material (80 to 100°). The results reported by Martinesi et al. [39] on samples nitrided at 400°C for 5 h are very

interesting because they show that the CA of a nitrided specimen compared to the one of an untreated sample can increase or decrease depending on the way it is cleaned before the measurements. For samples (untreated and nitrided) that was sonicated in acetone for 5 min. and dried in air, the contact angle increases from 73° to 82°, whereas for the set of samples subjected to a sterilization procedure and incubated with acetic acid, the CA passes from 73° to 71° (drop volume of 3 µl). Previous experiments [42] have shown that the initial CA measured immediately after sample 2 was polished was 45° and reach 60° after 10 days of air exposure (drop volume of 1 µl). Kim et al [43] have also report a spectacular change in surface wettability for polished and aged AISI STS 304 sample (from 40° to 100° after 40 days of air exposure for a drop volume of 5 µl). If this ageing effect has been known for quite a long time for plasmas treatments with Ar or O_2 [44], it is only very recently that it is taken into account during surface texturing by laser ablation [45]. A proposed explanation is the chemical adsorption of airborne organic compounds via the esterification between the carboxyl in the airborne organic compounds and the hydroxyl on the surface [45]. In this study, the effect of temperature is shown to be important. At moderate temperatures (< 200°C) airborne organic compounds adsorption is enhanced, which promotes the superhydrophobic character of the patterned surface. At higher temperatures (> 200°C) airborne organic compounds decrease and the patterned surface becomes hydrophilic. It must be noted that this ageing effect was not observed on the nitrided samples.

Borgioli et al. [31, 34, 39-40] have conducted interesting experiments on the wettability of nitrided AISI 316 L samples that underline the effects of bias of the samples being processed. Whatever the experimental conditions, the CA of the nitrided surfaces is always greater (78° to 98°) than that of the polished non-nitrided surface (70°-72° for a drop volume of 0.5 µl). For all samples, the CA is also found to decrease as the drop volume is higher (from 0.5 µl to 3 µl) [40]. In their latest experiments [31, 34], they carried out short nitriding treatments (8 to 10 min.) with different bias. These short treatments give larger CAs (94° to 104° for a drop volume of 0.5 µl) than those obtained for long treatments (84° to 88° to 380 ° C). This result remains unexplained. As discussed in the introduction, changing the bias voltage modify the ion bombardment giving different roughness to the treated surfaces. The higher the roughness of the nitrided surfaces are the higher the CAs are [31, 34, 40]. Such an explanation can be also be applied to the results gained by Aizawa et al. [41] in a transferred plasma with – 500 V of bias applied to a AISI 316 sample nitrided at 400°C for 2 h The CAs are 40° for the untreated sample and 104° for the nitrided one.

Figure 1 presents our preliminary results obtained for the wetting properties of AISI 316L samples 1 (table 2) nitrided at 400°C for different times ~~(table 1)~~. Some results reported from the literature and discussed before are also shown in this figure. It appears that the CA is always higher for all the nitrided samples as compared to a polished sample. However, large discrepancies are observed between our two sets of experiments. Our values for experimental set 1 are high (88° to 107°) and comparable to those reported by Borgioli et al. for short treatment times. However, our values for a short treatment time is comparable to the one of the untreated polished sample (60-62°). Starting from the same idea as Borgioli et al. we suspect the roughness of the nitrided sample to be responsible of the wetting properties. Left part of figure 2 shows that a honeycomb like structure exists at the surface of nitrided samples. However, there is no clear relation between roughness and contact angle as it can be seen from the right part of figure 2. Two polishing steps have been performed on the sample nitrided 4 h from set 2 with an initial CA of 88°. After a soft polishing intended to remove the relief induced by the nitriding treatment the CA was a little bit lower (86°). After the final polishing step, almost the 7 µm of total thickness of the nitrided layer was removed and the CA measured immediately after the polishing was 35°. In these preliminary experiments, it was not possible to finely control the surface topography by successive polishing of the nitrided surface.

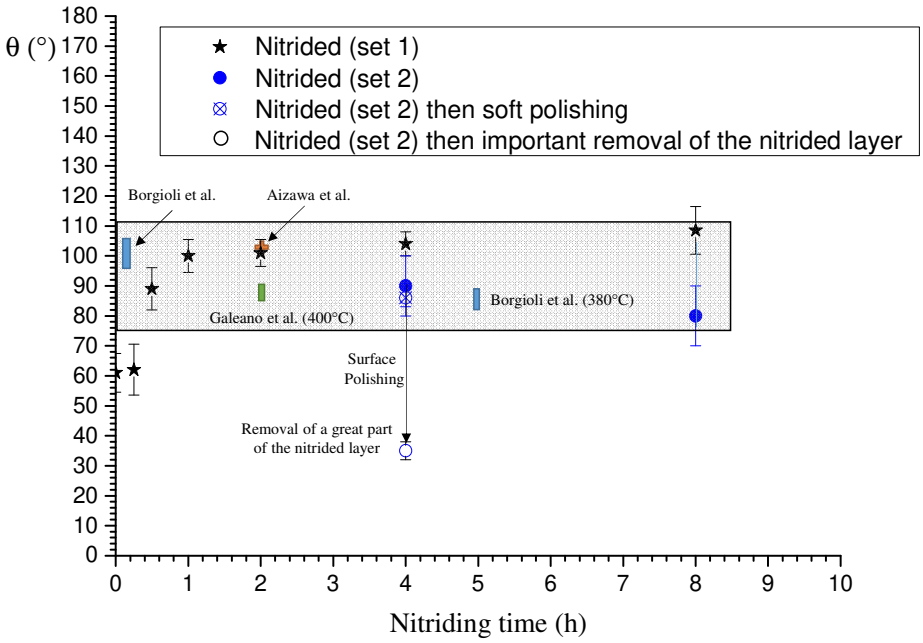

Figure 1: Evolution of the contact angle (drop volume 2-3 µl) as a function of nitriding time for AISI 316L sample 1 and for two sets of nitriding experiments at 400°C. The sample nitrided for 4 h for set 2 was polished two times after the nitriding treatment in order to see the influence of roughness. Results from the literature are also reported. The grey rectangle summarize the domain of contact angles for AISI 316L samples nitrided at low temperature (≤ 400°C).

For the partial wetting case, the spreading and evaporation kinetics are greatly influenced by the existence of CA hysteresis [46]. In addition to the sessile CA it exists dynamic CAs (i.e., the advancing and receding CAs). The dynamic CAs can be determined using two methods: the tilting plate and volume changing methods. In the first method, the drop is deposited on a plate, which is tilted to a critical angle known as the sliding angle for which the drop moves. The advancing and receding CAs are then measured as the angles on the downhill and uphill sides respectively. In the volume changing method, the advancing CA is measured as the maximum CA achieved by the drop as liquid is added prior to the outward movement of the drop. The receding CA is measured by withdrawing liquid from the drop to a point at which the drop begins to recede [46]. The difference between the advancing and receding CAs is known as contact hysteresis [46]. In our case it was not possible to measure the dynamic CAs due to the extremely strong pinning characteristics of our samples. It was even possible to reverse the sample with the droplets without any change in the droplets state.

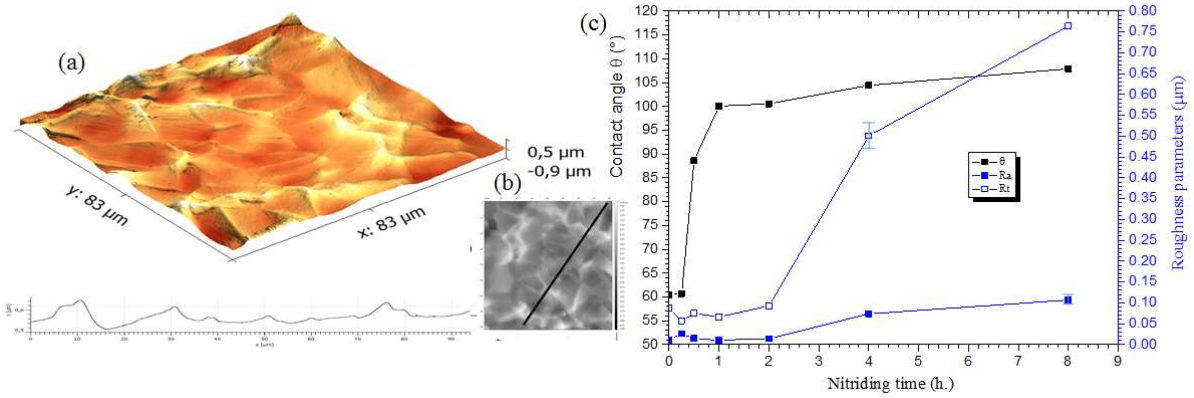

Figure 2: Left: (a) AFM 3D view of the sample nitrided for 8 h, extracted height profile (b) (c). Right: evolution of the contact angle (set 1 from figure 1) and of the roughness parameters as a function of nitriding time for AISI 316L sample 1 (total height of profile R_t and arithmetic mean roughness R_a).

During the evaporation of sessile drop ~~(see figure 3 for instance)~~ in the partial wetting case with contact hysteresis four possible evaporation steps are generally observed [47-49]. First an initial step or propagation step during this short initial spreading period (< 1 min.), the CA and the radius R change simultaneously to reach the initial considered values for the next step; stage I: the CA angle θ decreases while the radius R of the drop remains constant. This step is known as the constant contact radius evaporation mode (CCR). In this configuration, the triple line remains pinned (pinning mode). According to Brutin and Starov [14], the stable CAs at the beginning and at the end of stage 1 are respectively the advancing and the receding CAs; stage II: the CA remains constant while the radius R of the drop decreases. This step is known as the constant CA evaporation mode (CCA). In this configuration, the triple line moves (depinning mode), stage III: the contact angle θ and the radius R of the drop decrease until the droplet completely disappears (mixed regime). The main characteristic of partial wetting is the contact angle hysteresis, which results in the occurrence of stage II, when the drop edge is pinned.
The examination of the literature and these preliminary results have led us to reconsider our approach to the study of wettability and the evaporation of water drops on nitrided surfaces of austenitic stainless steels.

4. Experimental results

Figure 3 presents the evolution of the CAs and drop widths (2 R) for drops of 1 µl as a function of time for sample 2, 3 and M nitrided for 2 h at 400°C with different bias (0, - 50 and – 200 V). To our knowledge, it is the first time such evaporation data are reported for austenitic stainless steel.

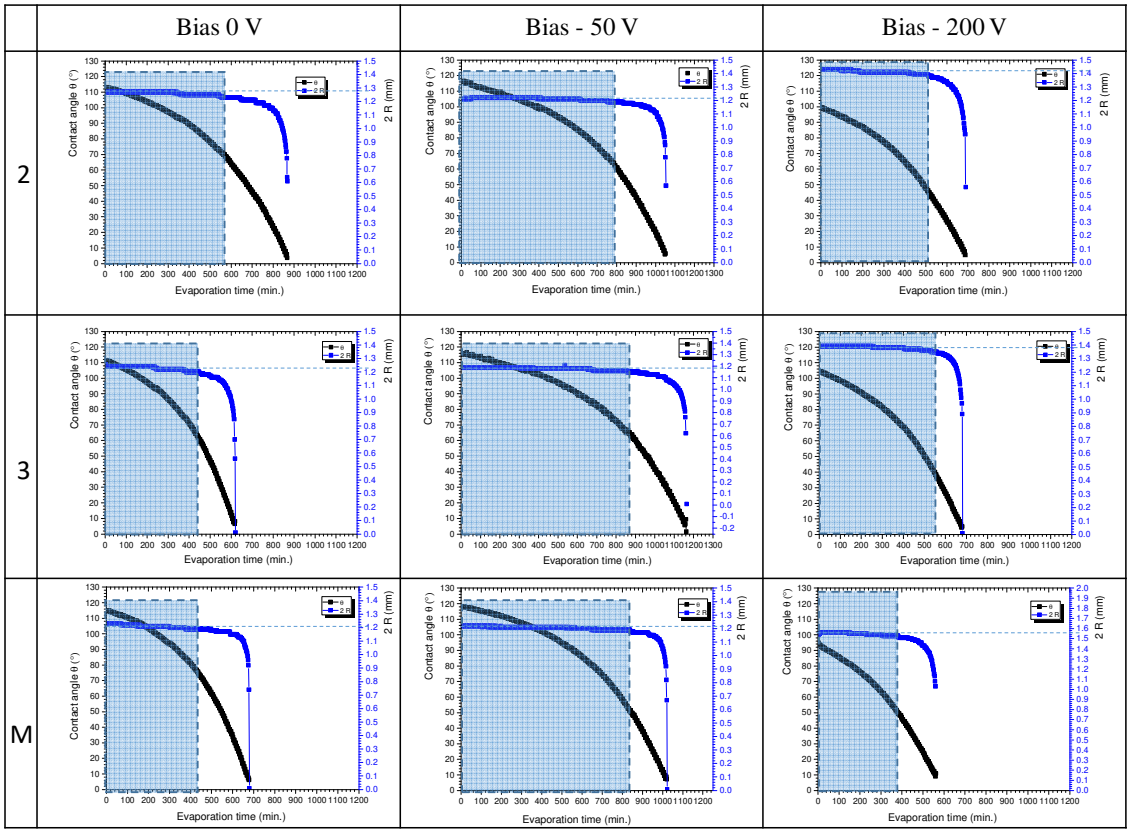

Figure 3: Evolution of the contact angle (θ) and drop width (2 R) as a function of evaporation time for drops of 1 µl as a function of time for sample 2, 3 and M nitrided for 2 h at 400°C with different bias (0, - 50 and – 200 V). The blue rectangles show the duration of the quasi-CCR regime.

Two different regimes for the evaporation can be distinguished from figure 3 on austenitic stainless steel nitrided samples: a quasi-constant diameter regime (designed after by quasi-CCR) and a mixed regime in which both diameter and CA are evolving with time. As reported before [42], sharp transitions from CCR to constant contact angle (CCA) are only observed for large volume drop. For drop volume less than 3 µl, a continuous transition from CCR to mixed regime is observed most of the time. As it can be seen on figure 3, apart from samples nitrided with a bias of – 50 V, the existence of pure CCR is open for debate and we will call it quasi-CCR mode. The time duration of the quasi-CCR regime is illustrated in figure 3 by blue rectangles. The evaporation time t_f is the time for which we measure the lowest CA. It can be seen that the ratio between the time duration of the quasi-CCR regime and the evaporation time t_f is more than 2/3. The CAs values at the end of the quasi-CCR can be considered as receding CAs according to Brutin and Starov [14]. Figure 4 represents the evolution of the initial values of CAs as a function of t_f for the experimental results presented in figure 3 but also from sputtering experiments. The elaboration conditions for the patterned sample are reported in reference [40]. The results presented for the polished samples are similar to those reported in [40] for sample 2. The lowest CA was obtained for measurements performed immediately after polishing and the CAs increase after 3, 7 and 10 days of air exposure (drop volume of 1 µl). It can be seen from figure 4 that nitrided and non-nitrided samples behave differently. The nitrided samples have both highest CAs and t_f as compared to non-nitrided samples. If a linear relationship seems clearly to emerge for non-nitrided samples, this is only partially the case for nitrided samples. We note in particular that the samples nitrided with a bias of - 50 V have a behavior different from the other samples. As shown by the results obtained on nitrided layers

with drop volumes of 0.6 and 0.3 µl, this linear trend is only valid for a given drop volume. At constant volume, higher evaporation times are obtained for higher initial CAs.

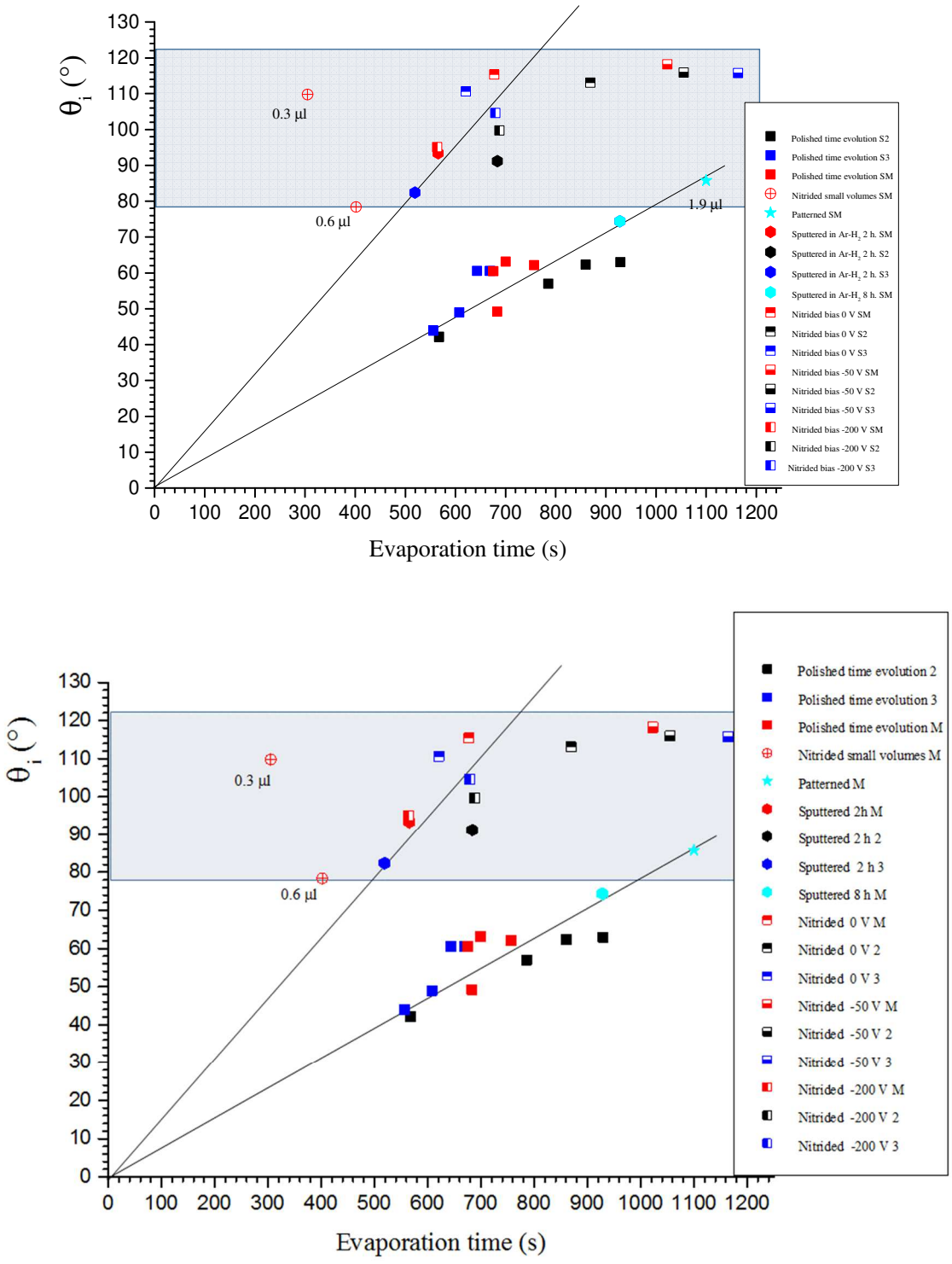

Figure 4: Evolution of the initial apparent CA (θ_i) as a function of the evaporation time for different AISI 316L samples. The drop volume is 1µl otherwise indicated. The blue rectangle shows the CA domain for nitrided samples. The lines are drawn to guide the eyes.

Figure 5 presents the droplet morphology on nitrided surfaces as observed by optical microscopy for samples 2, 3 and M. The drops show some anisotropy. The three-phase contact line (TPCL) is not strictly circular. Observations under optical microscopy of the trace left by the evaporation of the drops on the surfaces shows that the TPCL partially follows the grain boundaries.

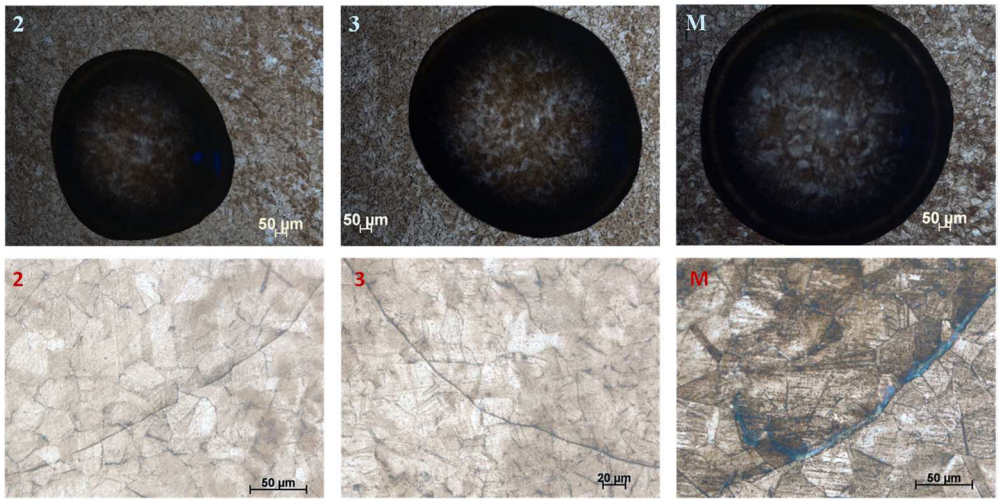

Figure 5: Droplet morphology on nitrided surfaces of samples 2, 3 and M. Top view: optical microscopy observation of water droplets. Bottom view: optical images of the traces remaining after the evaporation of water droplets.

Figure 6 shows SEM images of sample M nitrided for 2 h at 400°C with a bias of – 50 V observed at different magnifications with a tilt of 20° or without tilt. At low magnifications, the grains are easily observed because of the anisotropic uplift of the nitrided grains. This grains uplift is the result of the plastic deformation in the only free direction to compensate the high internal stresses during the formation of a specific metastable phase γ_N called expanded austenite occurring during nitriding treatment carried out below 420°C [30, 32, 33, 50]. Figure 6 also reveals the presence of very small particles which seed the nitrided surface. Figure 7 presents the results obtained by SEM at the same magnification on the samples nitrided with different bias. When there is no bias, a dense distribution of particles is observed, the size of which varies greatly from a few tens of nanometers to 200 nm. The particle size decreases from sample 3 to sample M and then to sample 2. When the bias is - 50 V, the distribution of particles is denser and the size of the particles is smaller (tens of nm) as compared to those observed on samples with no bias. The mean particle size is the highest for sample 3. In the case of samples biased at -200 V, practically no more particles are observed.
~~The SEM pictures in Figure 7 show only the places where the most particles are observed: practically no particles are observed. The particle density decreases from sample 3 to sample 2.~~
Particles on sample M are only present at grain boundaries.
Figure 8 presents cross section views of a FIB foil taken from the surface of a M-type sample nitrided for 8 h at 400 °C in a gas mixture of 80% N_2 - 20% H_2 with a bias of – 50 V and a pressure of 1 Pa. Over the nitrided layer, crystalized particles of a hundred of nm are detected. These particles are made up only of iron, nitrogen and oxygen and will be called oxynitrides hereafter.
Figure 9 gives an example of the procedure applied for the measurements of topographical parameters in the case of sample M sputtered for 2 h Undulation represents the topographic variations at the scale of grains (> 5 µm) and roughness represent variations at a scale less than 2 µm. For roughness measurements, we are at the limits of the spatial resolution of our device

(0.7 μm) with regard to the holes shown in the SEM picture of figure 9b. However, we do measure the roughness represented by white lines in figure 9d and lines in the SEM picture. We are unable to measure the oxynitrides particles with the white light interferometer. The obtained results are presented in table 3. For the undulation profile, S_{ku} (Kurtosis) values around 3 are obtained for all the samples. It means that the height distribution is normal: the parts of the profile in points are equal to the parts in the form of holes. The roughness parameters are more instructive, especially the S_{sk} (skewness) values which represent the degree of asymmetry of the roughness shape. For negative S_{sk} values, the height distribution is skewed below the mean plane and for positive S_{sk} values, the height distribution is skewed above the mean plane. Figure 10 presents the evolution of initial CAs as a function of S_{sk} values for roughness obtained after the application of a robust Gaussian filter. Apart from samples nitrided with a bias of – 50 V an interesting linear correlation is found.

5. Discussion

When working on the wettability of rough surfaces the two most popular models are the Wenzel model (relation 1) and the Cassie-Baxter model (relation 2) [2-3, 14-16].

$$\cos \theta_w = r_w \cos \theta_0 \quad (1)$$

$$\cos \theta_{CB} = \phi_s (\cos \theta_0 + 1) - 1 \quad (2)$$

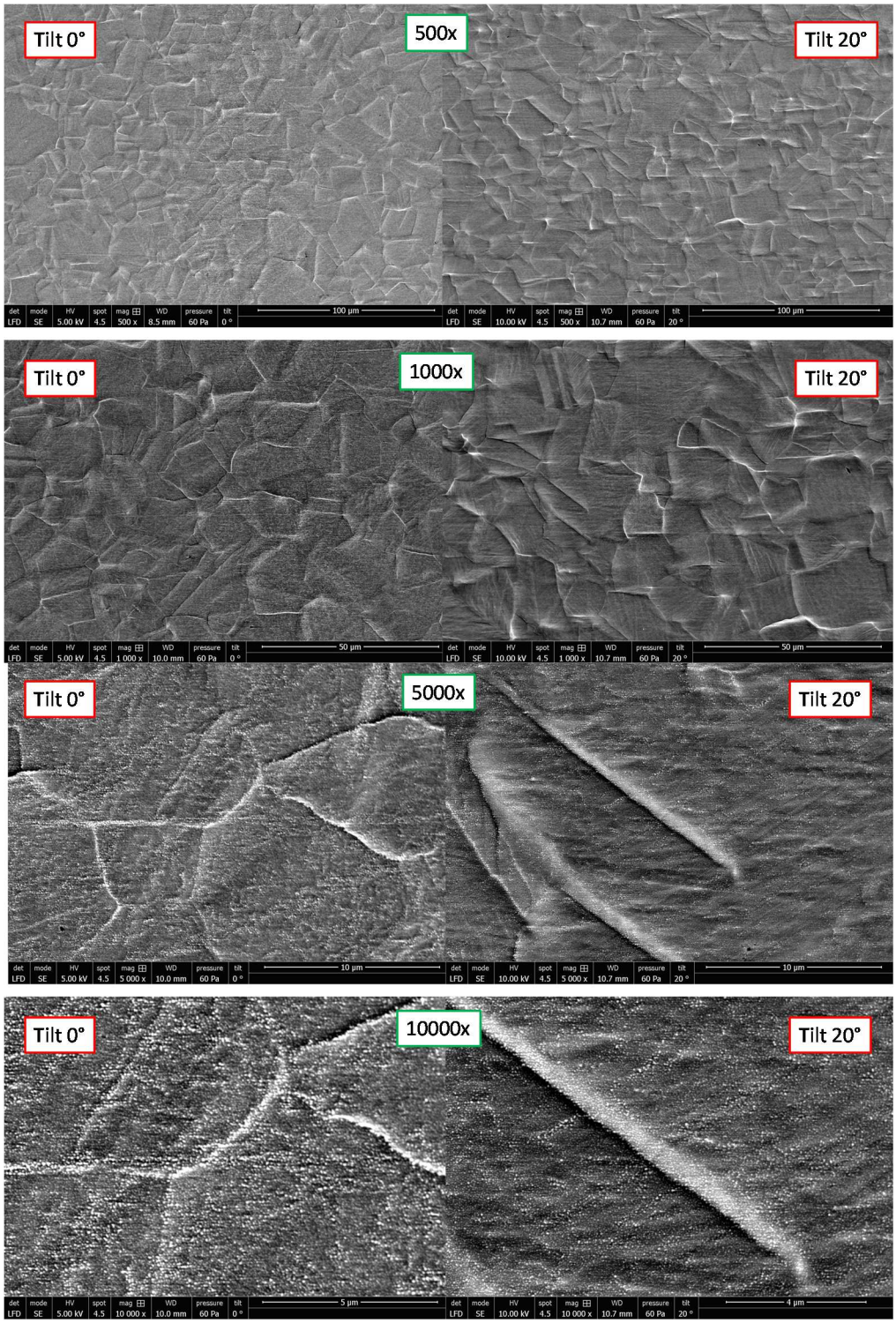

Figure 6: SEM images of sample M nitrided for 2 h at 400°C with a bias of – 50 V observed at different magnifications with a tilt of 20° or without tilt.

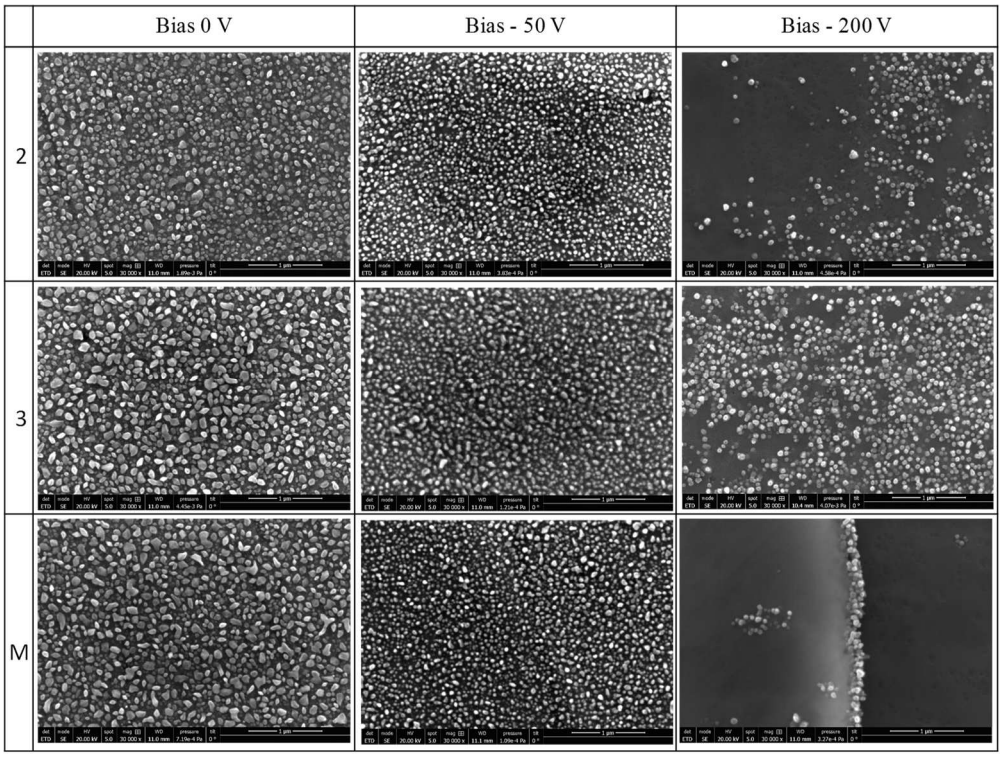

Figure 7: SEM images at the same magnification of the surface of the three samples nitrided for 2 h at 400°C with bias of 0, – 50 and – 200 V. For the - 200 V bias, the presented results are for places where the particles are more numerous.

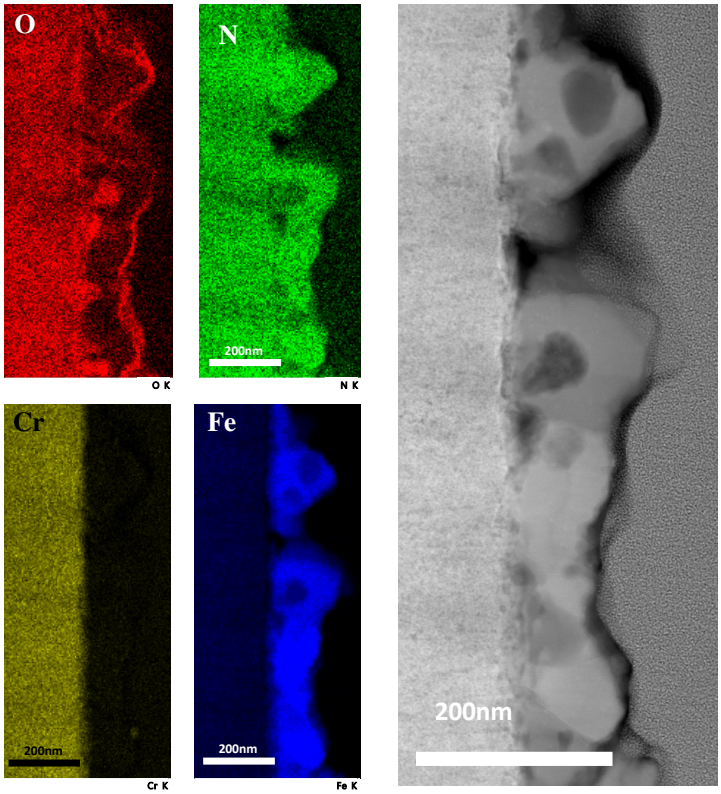

Figure 8: Cross section views of a FIB foil taken from the surface of a M-type sample nitrided for 8 h at 400 °C (gas mixture 80% N_2 - 20% H_2, bias - 50V, pressure 1 Pa). On the left, distribution of the elements (Cr, Fe, N, O) in STEM-EDS, on the right STEM-HAADF image.

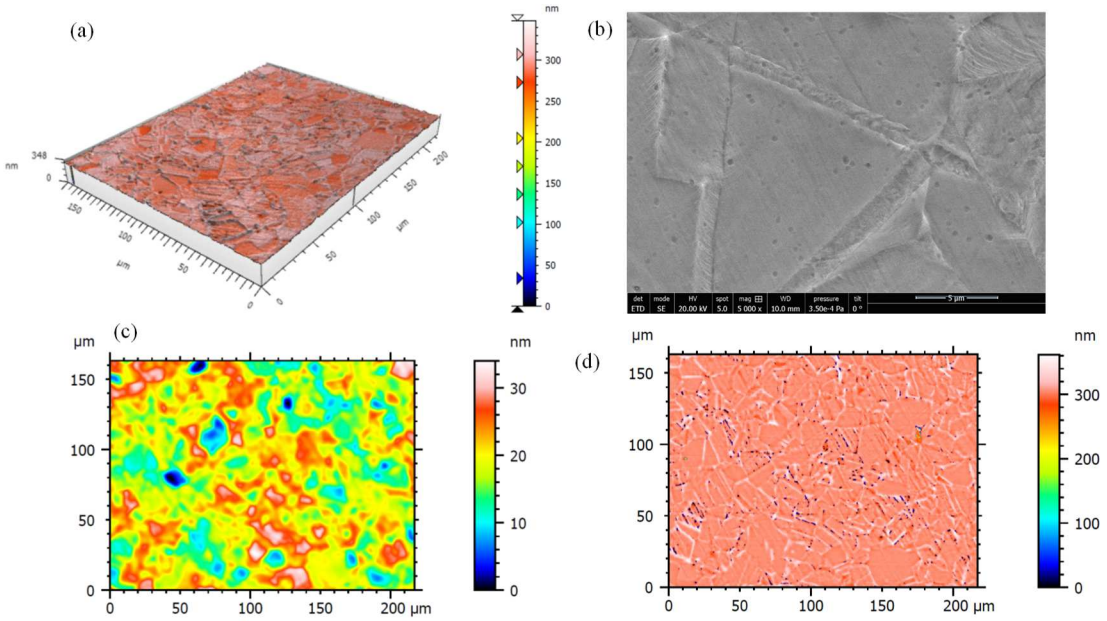

Figure 9: Roughness measurements procedure for sample M sputtered for 2 h (a) original 3D profile after the application of the filter, (b) SEM picture, (c) undulation profile and (d) roughness profile.

	Nit 0 V 2	Nit 0 V 3	Nit 0 V M	Nit -50 V 2	Nit -50 V 3	Nit -50 V M	Nit -200 V 2	Nit -200 V 3	Nit -200 V M	Sput. 2 h -100 V 2	Sput. 2 h - 100 V 3	Sput. 2 h -100 V M
S_q (µm)	0.001	0.014	0.021	0.079	0.084	0.108	0.183	0.135	0.182	0.029	0.014	0.03
S_a (µm)	0.003	0.005	0.007	0.052	0.054	0.047	0.009	0.065	0.095	0.007	0.004	0.008
S_{sk}	25	18	12.3	1.27	2.11	1.02	1.93	1.72	1.43	- 9.24	- 16.2	- 8.27
S_{ku}	733	384	175	8.26	11.7	12.1	14.8	15.5	11.6	91.6	326	72.7
S_p (µm)	0.309	0.345	0.332	0.579	0.735	0.806	1.75	1.46	1.57	0.057	0.068	0.059
S_v (µm)	0.03	0.033	0.0325	0.425	0.370	0.418	0.912	0.711	0.755	0.309	0.30	0.303
S_z (µm)	0.337	0.378	0.364	1	1.11	1.22	2.66	2.17	2.22	0.367	0.370	0.362

Table 3. Roughness topographical parameters of different AISI 316L stainless steel samples (S_q: root mean square height, S_a: arithmetical mean height, S_{sk}: skewness, S_{ku}: kurtosis, S_p: maximum peak height, S_v: maximum pit height, $S_z = S_p + S_v$). Uncertainties are 3-4% for S_q, 6-8% for S_a, 4-6% for S_{sk} and Sku and 4-6% for S_p, S_v and S_z.

In these relations, θ_0, θ_w and θ_{CB} are respectively the Young CA measured on a flat surface, the Wenzel CA and the Cassie-Baxter CA, r_w is the ratio of the solid-liquid interfacial area to the projected interfacial area and ϕ_s is the ratio of solid-liquid interfacial area to the total interfacial area. The Wenzel relation is used when the liquid completely penetrates into the asperities (homogeneous wetting regime). The Cassie-Baxter relation can be used for chemically heterogeneous surfaces (two components), relation 2 is for the situation of air pockets present between the surface and the liquid. Relation 1 and 2 were derived from thermodynamically considerations under the assumption that the energy loss at a moving TPCL can be neglected when a liquid droplet reaches an equilibrium state on a solid surface. However, energy losses at the TPCLs have been largely reported [51-54]. According to Wenzel's equation, when the roughness increases, the CA increases for hydrophobic surfaces ($\theta_0 > 90$ °) but decreases for hydrophilic surfaces ($\theta_0 < 90$ °). This is generally not verified for hydrophilic surfaces. Some models try to take into account the energy loss at the TPCL [54-56]. The Kang-Jacobi model allows to lower the value of the transition angle between hydrophilic and hydrophobic states to

48 ° [55] or even 43 ° [54]. Apart from the case of nitrided layers having oxynitrides on the surface, none of the relations 1 and 2 is able to explain our wettability results. As a matter of fact, the traces left by the TPCL at the end of evaporation (figure 5) suggest that there is no air pockets in the space formed at the scale of grains between the extruded grain boundaries. Hence equation 2 is not applicable. From our surface topography measurements, we can estimate the value of factor rw in equation 1. It is very close to 1 and, as a consequence, equation 1 is not able to explain why θ_w (the contact angle of topographically modified nitrided surfaces) is higher that θ_0 (the angle corresponding to a flat nitrided surface). Although the CA of a flat nitrided surface is not yet available, figure 1 suggest it can be less than a non nitrided flat surface. We must turn to the pinning phenomenon to try to explain our observations. The current understanding of the TPCL pinning phenomenon is based on the Gibbs' criterion (relation 3), which is illustrated in Figure 11a [57-60].

$$\theta_c = \theta_0 + \alpha \qquad (3)$$

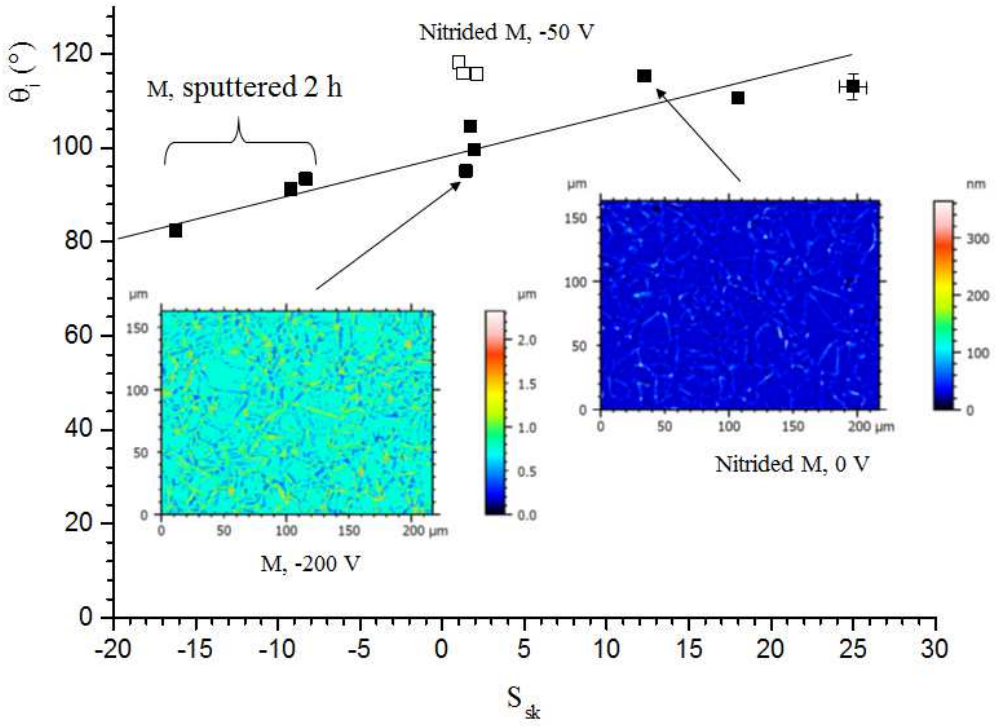

Figure 10: Initial values of CAs as a function of S_{sk} value obtained from the roughness profiles on samples M treated in different conditions (table 2). A robust gaussian filter was applied to the data.

In this relation, θ_c is the critical angle for depinning and $\pi - \alpha$ is the angle of the apex formed by the substrate faces. The Gibbs' criterion stipulates that the contact angle at the edge of surface with a negative slope can take any value between θ and $\theta + \alpha$, if the horizontal direction is considered as the reference one. Pinning of the contact line from the edge occurs when $\theta < \theta_c$, while depinning occurs when $\theta > \theta_c$. As illustrated in figure 11b, such a constraint does not exists when the TPCL meet a surface with a positive slope. On sharp edges, that are associated to energy barriers for the spreading of droplets, energy is stored in the pinned droplet. Such a concept is to be connected to the energy loss at the TPCL taken into account in modelling [54-56]. One might think that the parameters, S_p, S_v and S_z are relevant parameters, but it is not. Only the asymmetry of the profile is important to determine the value of the contact angle.

Thus, the CAs are higher for an asymmetrical profile with more peaks than valleys. The height of peaks and valleys does not seem to play an important role. We can therefore conclude that the wettability of nitrided surfaces does not depend on the flatness of the grains but is very sensitive to localized peaks present at the grain boundaries. Thus, the CAs are higher for an asymmetrical profile with more peaks than valleys. The TPCL is not following grain boundaries but is pinned to these localized peaks as suggested by figure 5. Although we have not presented analysis of the nitrided surface topography parameters for which the contact angles are less than 90°, we believe that it is possible to obtain such topographic configurations for nitrided layers. Indeed, according to the nature of the coupling between the deformations of surfaces induced by nitriding and their sputtering by ion bombardment, it must be possible to obtain a wide range of S_{sk} values and thus of CAs. This hypothesis should be tested in future experiments.

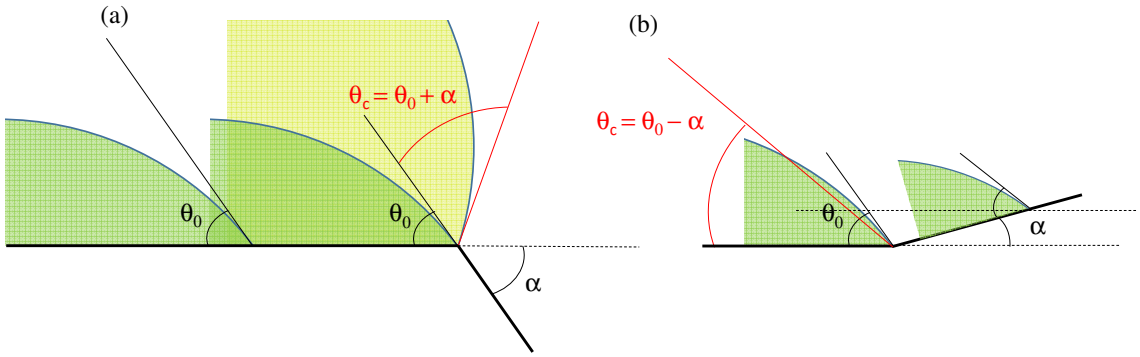

Figure 11: Illustration of the Gibbs' criterion for a droplet in contact with a surface with (a) a positive slope and (b) a negative slope.

It is clear from figures 6 and 7 that the small oxynitride particles, present at the surface of the nitrided layer, have a strong influence on the CAs values. Their shape, size and distribution make possible an air trapping effect leading to a kind of fakir state as described by the Cassie-Baxter relation 2. Thus it is coherent that when the particles are no longer present in sufficient numbers or when their density decreases (in the case of nitrided samples with a bias of - 200 V), the CAs change from 110-118° to 95-106°. Such sub-micrometric particles have already been observed during PANTs [34, 61-63]. The only explanation given for the origin of this particles are deposition of metallic species resulting from sputtering of the worktable in steel. This is perhaps true in the so called active screen plasma nitriding (ASPN) process in which a negative bias voltage (up to - 900 V) is applied to a metal mesh screen surrounding the piece to be treated. Li and co-worker have observed by HRTEM a composite duplex layer formed by an amorphous and nano-crystallized oxynitrided upper layer over a nitrided layer on austenitic stainless steel AISI 304 oxynitrided at 440°C for 16 h in a NH3 atmosphere with 2% of oxygen [62-63]. It is not the purpose of this paper to explain the origin of the sub-micrometric particles we observed, but we can say that it most probably result from a selective oxidation of the nitrided layer due to very slow oxygen desorption coming from water vapour adsorbed on the wall during opening of the reactor.

The volume variation for droplets small enough to be associated with spherical caps (the radius R of the drop is less than the capillary length: 2.7 mm for water) is given by [3]:

$$\frac{dV}{dt} = \frac{\pi R^3}{(1+\cos\theta)^2}\frac{d\theta}{dt} + 3\pi R^2 g(\theta)\frac{dR}{dt} \quad \text{with} \quad g(\theta) = \frac{\cos^3\theta - 3\cos\theta + 2}{3\sin^3\theta} \qquad (4)$$

In the CCR regime, Popov [3] has shown that equation (4) can be expressed by:

$$\frac{dV}{dt} = -\pi R \frac{D(C_\infty - C_S)}{\rho} f(\theta) \text{ with } f(\theta) = \frac{\sin\theta}{1+\cos\theta} + 4\int_0^\infty \frac{1+\cosh 2\theta\tau}{\sinh 2\pi\tau} \tanh[\tau(\pi - \theta)]d\tau \quad (5)$$

ρ is the fluid density, $f(\theta)$ is a function of the contact angle θ, D is the diffusion constant for vapour in air, C_S is the vapour saturation concentration just above the liquid-air interface, C_∞ is the ambient vapour concentration. This last relation is relevant for all the θ values. When $\theta \rightarrow 0$, relation (5) gives [3]:

$$\theta = \theta_i \left(1 - \frac{t}{t_f}\right) \text{ and } V = \frac{\pi R_i^3 \theta_i}{4}\left(1 - \frac{t}{t_f}\right) \quad (6)$$

$$t_f^{CCR} = \frac{\pi \rho R_i^2 \theta_i}{16 D (C_\infty - C_S)} \quad (7)$$

In relations (6) and (7), θ_i is the initial contact angle and t_f^{CCR} is the evaporation time in the CCR regime. Relation (5) has no simple analytical solutions but some analytical expression have been proposed for $f(\theta)$ [64]. The results for the CCR mode can be found in [42]. As a general rule, the simple evaporation model gives the following power law for the droplet volume evolution as a function of time (V_i is the initial volume of the droplet):

$$\left(\frac{V}{V_i}\right)^\beta = \left(1 - \frac{t}{t_f}\right) \quad (8)$$

Works from Nguyen et al [64] and Hu et al [65] show that the β factor is evolving between 1 and 2/3 for the CCR mode and is equal 2/3 for the CCA mode.

From our results (figure 3) it can be seen that the evolution of the apparent contact angle is not a linear function of time as predicted by relation 6. Figure 12 shows the evolution of the logarithm of the normalized drop volume ($V_{norm} = V/V_i$, where V_i is the initial volume of the droplet) as a function of ln $(1 - t/t_f)$ for nitrided sample M with different bias. During most of the evaporation process, the evolution of ln V_{norm} as a function of ln $(1 - t/t_f)$ is linear for these samples and for all the other samples (slops between 1.08 and 0.9 and around 0.8 for smaller droplet volumes). So it can be concluded that the volume evolution with time given by relation (6) for the evaporation in the CCR mode is effective in both cases. In other words, we find a value $\beta = 1$ for the relation 8. Some deviations are observed for the final part of the evaporation process.

Figure 13 is intended to show to what extent relation 7 is valid. It is remarkable to note that it describes a very large number of cases well, except the three samples nitrided with a bias of - 50 V, the sample 2 nitrided with no bias of and the sample sputtered in Ar for 8 h. Figure 7 shows that the average particle size is smaller in the case of the nitrided samples with a bias of - 50 V, as well as for the sample 2 nitrided without bias than in the case of the samples 3 and M nitrided without bias.

We believe that the differences in both the size and a shape of the particles explain the difference in evaporation times between these two batches of samples. These differences in the iron oxynitride particles therefore plays an important role in the evaporation of the water drops on the nitrided surfaces. The smaller and denser they are, the longer the evaporation time. As it can be seen on figure 3, the time duration of the CCR regime is longer for nitrided surfaces at - 50 V. It can be postulated that the pinning of the triple line is much more important on the

particles of iron oxynitride resulting from a nitriding treatment with samples biased at -50 V.

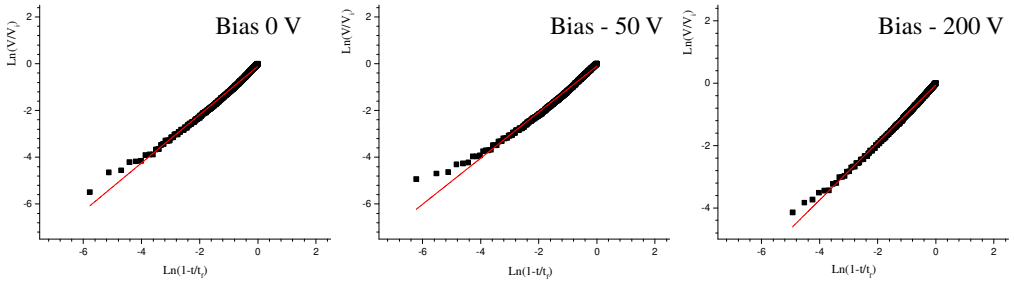

Figure 12: Evolution of the logarithm of the normalized droplet volume as function of the logarithm of (1- t/t_f) for nitrided sample M with different bias.

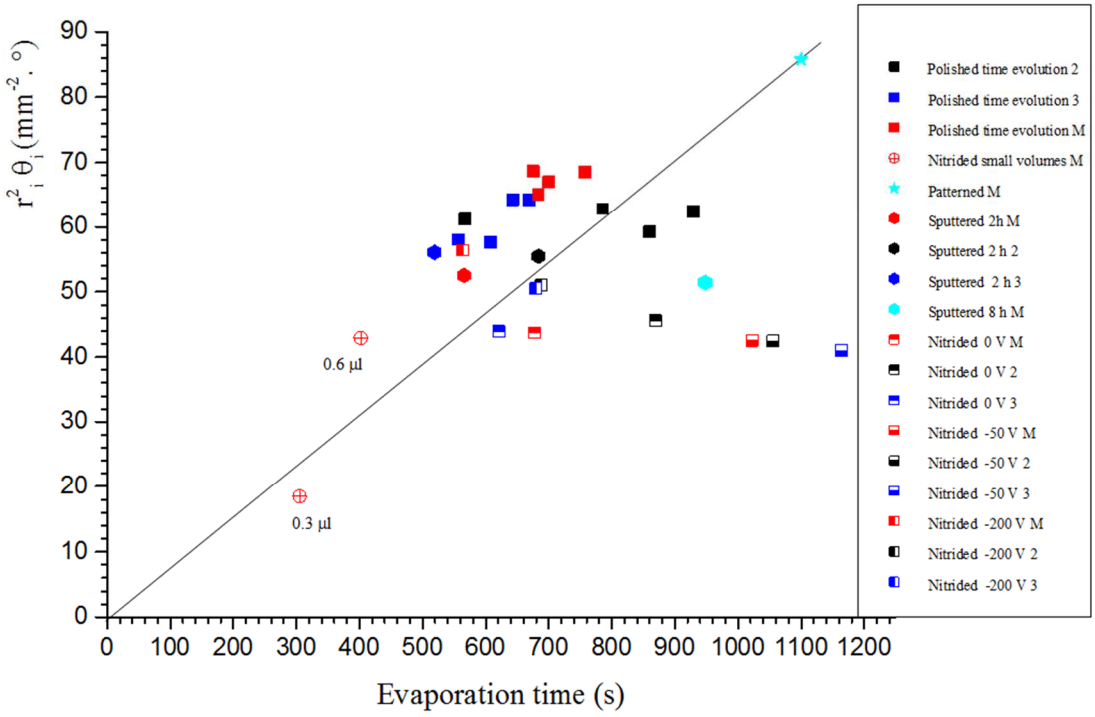

Figure 13: Evolution of $R_i^2\theta_i$ as function as a function of the evaporation time for different AISI 316L samples. The drop volume is 1µl. The line is drawn to guide the eyes. Uncertainties in $R_i^2\theta_i$ can be estimated to be at least between 12 and 15%.

5. Conclusion

A nitriding treatment of metallic materials can provide better durability to processed surfaces. Nitriding at low temperature (< 420°C) of stainless steels, such as AISI 316L, produces a surface layer consisting of highly stressed expanded austenite which leads to surface deformation at the grain boundaries. Although the wettability of nitrided surfaces is of great importance, it is poorly studied. Preliminary experiments and the examination of the results reported in the litterature have shown dispersed results. Topography is suspected to play an important role but no direct relation between roughness and wetting parameters is available. In this study, the use of a transferred plasma for nitriding provides independent substrate biasing

giving the opportunity to tailor the surface before and during the nitriding treatments. The effect of different treatments, effectively done during a nitriding treatment, were studied. A cleaning pre-treatment (Ar-H2 plasma) produces topographical modifications of the surface by selective sputtering of the grains giving contact angles between 80 and 90 °. Nitriding treatments are carried out with no (0 V) or high bias voltage (- 200 V) give higher initial contact angles θ_i. We found that the asymmetry of the surface topographies is an important parameter to describe the surface wettability, not only nitrided surfaces, but also other surfaces such as powder-coated surfaces. A linear relation between the initial contact angle θi and the skewness (S_{sk}) topographical roughness parameter was found for all of these surfaces. Ion bombardment produces hole at the surface associated to negative S_{sk} values (surface with more valley than picks). During relatively long nitriding treatments (more than one hour), the very high internal stresses generated by very high nitrogen incorporation produce anisotropic deformations of the austenite grains which lead to the formation of spikes at the grain boundaries giving surfaces with positive S_{sk} values. Pinning of the three-phase contact line on peaks localized at grain boundaries are responsible for the reported high contact angles. Concerning the evopration, even if the initial contact angle is higher than on non-nitrided and polished surfaces, the evaporation time of the drops is not higher than on non-nitrided and polished surfaces. A tailoring of the nitriding parameters is possible to obtain a desired results in terms of wetting. The theory for evaporation in the constant contact radius (CCR) mode, which states that the evaporation time is proportional to $R_i^2\theta_i$, the square of the initial contact radius times the initial contact angle is verified in many cases except for nitrided samples covered by nanoparticles.
We have shown that the presence of iron oxynitride particles having a size of tens of nanometers and densely distributed on the surface increases both the initial contact angle (up to 118°) and the evaporation time. It was shown that the presence of these particles can be controlled by changing the ion bombardment through the bias voltage applied to the substrates. In order to optimize the performance in evaporation, it would be necessary to better control the parameters leading to the formation of these particles. Even if they do not make it possible to improve the performance in evaporation, nitriding treatments make it possible to greatly improve the durability of textured surfaces without degrading the performance in evaporation.

Acknowledgments

This work and the post-doctoral stay of S. Tsareva were supported by the French Government through the programs Institut Carnot ICÉEL, and “Investissements d’avenir” operated by the French National Research Agency (ANR) and referenced to as ANR-11-LABX-0008-01 (LabEx DAMAS).
This work was supported by the French Government through the programs Institut Carnot ICÉEL, and “Investissements d’avenir” operated by the French National Research Agency (ANR) and referenced to as ANR-11-LABEX-0008-01 (LabEx DAMAS).

References

[1] R. Picknett, R. Bexon , the evaporation of sessile or pendant drops in still air, J. Colloid Interface Sci., 61 (1977) 336–350.
[2] H.Y. Erbil, Evaporation of pure liquid sessile and spherical suspended drops, Adv. Colloid Interface Sci., 170 (2012) 67-86.
[3] Y.O. Popov, Evaporative deposition patterns: spatial dimensions of the deposit, Phys. Rev. E, 71 (2005) 036313.

[4] Y. Sun, Z. Guo, Recent advances of bioinspired functional materials with specific wettability: from nature and beyond nature Nanoscale Horiz., 2019, 4, 52, (https://doi.org/10.1039/c8nh00223a)
[5] B. Bhushan, Y.C Jung, Natural and biomimetic artificial surfaces for superhydrophobicity, self-cleaning, low adhesion, and drag reduction, Progress in material Science 56 (2011) 1-108. (https://doi.org/10.1016/j.pmatsci.2010.04.003)
[6] M.J. Kreder, J. Alvarenga, P. Kim, J. Aizenberg, Design of anti-icing surfaces: smooth, textured or slippery?, Nature Reviews Materials, 1 (2016) 1-15.
[7] O. I. Vinogradova, A. L. Dubov, Superhydrophobic textures for microfluidics, Mendeleev Commun., 2012, 22, 229–236.
[8] P. Tao, W. Shang, C. Song, Q. Shen, F. Zhang, Z. Luo, N. Yi, D. Zhang, T. Deng, Bioinspired Engineering of Thermal Materials, Adv. Mater., 27 (2015) 428-463.
[9] Y. Lu, Superior lubrication properties of biomimetic surfaces with hierarchical structure, Tribology International 119 (2018) 131–142.
[10] A. Fihri, E. Bovero, A. Al-Shahrani, A. Al-Ghamdi, G. Alabedi, Recent progress in superhydrophobic coatings used for steel protection : A review, Colloids and Surfaces A: Physicochemical and Engineering Aspects 520 (2017) 378–390
[11] P. Zhang, F.Y. Lv, A review of the recent advances in superhydrophobic surfaces and the emerging energy-related applications, Energy 82 (2015) 1068-1087.
[12] M. Edalatpour, L. Liu, A.M. Jacobi, K.F. Eid, A.D. Sommers, Managing water on heat transfer surfaces: A critical review of techniques to modify surface wettability for applications with condensation or evaporation, Applied Energy 222 (2018) 967–992.
[13] D. Attinger, C. Frankiewicz, A.R. Betz, T.M. Schutzius, R. Ganguly, A. Das, C.J Kim, C. M. Megaridis, Surface engineering for phase change heat transfer: A review, MRS Energy & Sustainability 1 (2014), 1-40.
[14] D. Brutin, V. Starov, Recent advances in droplet wetting and evaporation, Chem Soc Rev. 47 (2018) 558-585. doi: 10.1039/c6cs00902f.
[15] J.W. Drelich, J. Boinovich, E. Chibowski, C. Della Volpe, L. Hołysz, A. Marmur, Contact angles: history of over 200 years of open questions, surface Innovations 8 ((2020) 3–27, (https://doi.org/10.1680/jsuin.19.00007).
[16] A. Marmur, C. Della Volpe, S. Siboni, A. Amirfazli, J.W. Drelich, contact angles and wettability: towards common and accurate terminology. Surface Innovations 5 (2017) 3–8, (http://dx.doi.org/10.1680/jsuin.17.00002)
[17] N. Cohen, A. Dotan, H. Dodiuk & S. Kenig, Superhydrophobic Coatings and Their Durability, Materials and Manufacturing Processes, 31 (2016) 9, 1143-1155. (https://doi.org/10.1080/10426914.2015.1090600)
[18] H.A. Abdel-Aal, functional surfaces for tribological applications: inspiration and design, Surf. Topogr., 4 (2016) 043001,(https://doi.org/10.1088/2051-672X/4/4/043001)
[19] X. Tian, T. Verho, R.H.A. Ras, moving superhydrophobic surfaces toward real-world applications, Science 352 (2016) 142-143, (http://dx.doi.org/10.1126/science.aaf2073)
[20] A. Milionis, E. Loth, I.S. Bayer, recent advances in the mechanical durability of superhydrophobic materials, Advances in Colloid and Interface Science 229 (2016) 57–79, (http://dx.doi.org/10.1016/j.cis.2015.12.007)
[21] V. Mortazavi, M.M. Khonsari, On the degradation of superhydrophobic surfaces: a review, Wear, 372-373 (2017) 145–157. (http://dx.doi.org/10.1016/j.wear.2016.11.009)
[22] L.R.J. Scarratt, U. Steiner, C. Neto, a review on the mechanical and thermodynamic robustness of superhydrophobic surfaces, Advances in Colloid and Interface Science 246 (2017) 133–152, (http://dx.doi.org/10.1016/j.cis.2017.05.018)

[23] X. Zhang, J. Mo, Y. Si, Z. Guo, How does substrate roughness affect the service life of a superhydrophobic coating? Applied Surface Science 441 (2018) 491–499, (https://doi.org/10.1016/j.apsusc.2018.01.232)
[24] A. Pavlik, G. Marcos, M. Coulibaly, J. Vincent, T. Czerwiec, S. Philippon, Improving the surface durability of patterned AISI 316LM steels by nitriding treatment for dry friction sliding, Tribology International 146 (2020) 106232 (https://doi.org/10.1016/j.triboint.2020.106232)
[25] T. Czerwiec, H. Michel, E. Bergmann, Low-pressure, high-density plasma nitriding: mechanisms, technology and results, Surf. Coat. Technol., 108-109 (1998) 182-190. (https://doi.org/10.1016/S0257-8972(98)00555-6)
[26] H. Michel, T. Czerwiec, M. Gantois, D. Ablitzer, A. Ricard, Progress in the analysis of the mechanisms of ion nitriding, Surf. Coat. Technol. 72 (1995) 103.
[27] H. Dong, S-phase surface engineering of Fe–Cr, Co–Cr and Ni–Cr alloys. Int. Mater. Rev. 55 (2010) 65–98.
[28] J. Baranowska, Importance of surface activation for nitrided layer formation on austenitic stainless steel. Surf. Eng., 26 (2006) 293–298.
[29] T. Czerwiec, H. He, S. Weber, C. Dong, H. Michel, On the occurrence of dual diffusion layers during plasma-assisted nitriding of austenitic stainless steel. Surf. Coat. Technol. 200 (2006) 5289–5295, (https://doi:10.1016/j.surfcoat.2005.06.014)
[30] F. Borgioli, from austenitic stainless steel to expanded austenite - S phase: formation, characteristics and properties of an elusive metastable phase, Metals, 10 (2020) 187. (https://doi:10.3390/met10020187)
[31] F. Borgioli, E. Galvanetto, T. Bacci, Surface modification of austenitic stainless steel by means of low pressure glow-discharge treatments with nitrogen. Coatings, 9 (2019) 604, https://doi:10.3390/coatings9100604
[32] T. Czerwiec, H. He, G. Marcos, T. Thiriet, S. Weber, H. Michel, fundamental and innovations in plasma assisted diffusion of nitrogen and carbon in austenitic stainless steels and related alloys, Plasma Proc. and Pol. 6 (2009) 401.
[33] T. Czerwiec, A. Andrieux, G. Marcos, H. Michel, Ph Bauer, « Is “expanded austenite” really a solid solution? Mössbauer observation of an annealed AISI 316L nitrided sample”, Journal of Alloys and Compounds 811 (2019) 151972.
[34] F. Borgioli, E. Galvanetto, T. Bacci, Effects of surface modification by means of low temperature plasma nitriding on wetting and corrosion behavior of austenitic stainless steel, Coatings 10 (2020) 98; (https://doi:10.3390/coatings10020098)
[35] Y.H. Lin, W.C Lan, K.L. Ou, C.M. Liu, P.W Peng, Hemocompatibility evaluation of plasma-nitrided austenitic stainless steels at low temperature. Surf. Coat. Technol. 206 (2012) 4785–4790, (https://doi:10.1016/j.surfcoat.2012.03.089)
[36] J. Buhagiar, T. Bell, R. Sammons, H. Dong, Evaluation of the biocompatibility of S-phase layers on medical grade austenitic stainless steels. J. Mater. Sci. Mater. Med. 22 (2011) 1269–1278, (https://doi:10.1007/s10856-011-4298-3)
[37] D.S. Galeano-Osorio, S. Vargas, J.M. Vélez, A. Mello, M.N. Tanaka, C.E. Castano, Hemocompatibility of plasma nitrided 316L stainless steel: Effect of Processing Temperature. Appl. Surf. Sci. 144704 (2019) (https://doi:10.1016/j.apsusc.2019.144704)
[38] J.K.F.S. Braz, G.M. Martins, V. Sabino, J.O. Vitoriano, C.A.G Barboza, A.K.M.C. Soares,; H.A.O. Rocha, M.F. Oliveira, C. Alves Júnior, C.E.B. Moura, Plasma nitriding under low temperature improves the endothelial cell biocompatibility of 316L stainless steel. Biotechnol. Lett. 41 (2019) 503–510, (https://doi:10.1007/s10529-019-02657-7)
[39] M. Martinesi, M. Stio, C. Treves, F. Borgioli, Biocompatibility studies of low temperature nitrided and collagen-I coated AISI 316L austenitic stainless steel. J. Mater. Sci. Mater. Med. 24 (2013) 1501–1513, (https://doi:10.1007/s10856-013-4902-9).

[40] F. Borgioli, E. Galvanetto, T. Bacci, Influence of surface morphology and roughness on water wetting properties of low temperature nitrided austenitic stainless steels. Mater. Charact. 95 (2014) 278–284, (https://doi:10.1016/j.matchar.2014.07.006).
[41] T. Aizawa, H. Morita, K. Wasa, low-temperature plasma nitriding of mini-/micro-tools and parts by tabletop system, Appl. Sci. 9 (2019) 1667, (https://doi:10.3390/app9081667).
[42] T Czerwiec, S Tsareva, A Andrieux, G A Bortolini, P H Bolzan, G Castanet, M Gradeck, G Marcos, thermal management of metallic surfaces: evaporation of sessile water droplets on polished and patterned stainless steel, IOP Conf. Series: Materials Science and Engineering 258 (2017)(https://doi:10.1088/1757-899X/258/1/012003).
[43] Kim D, Kim J, Chu C N, 2016, Aging effect on the wettability of stainless steel, Materials Letters 170, 18–20, (https://doi.org/10.1016/j.matlet.2016.01.107).
[44] M. Mantel, J.P. Wightman, influence of the surface chemistry on the wettability of stainless steel, Surf. Interface Anal. 1994, 21, 595–605, (https://doi:10.1002/sia.740210902).
[45] X. Li, Y. Jiang, Z. Jiang, Y. Li, C. Wen, J. Lian, reversible wettability transition between superhydrophilicity and superhydrophobicity through alternate heating-reheating cycle on laser ablated brass surface, Applied Surface Science 492 (2019) 349–361, (https://doi.org/10.1016/j.apsusc.2019.06.145).
[46] C. H. Kung, P. K. Sow, B. Zahiri, W. Mérida, Assessment and Interpretation of Surface Wettability Based on Sessile Droplet Contact Angle Measurement: Challenges and Opportunities, Adv. Mater. Interfaces 6 (2019) 1900839.
[47] H. Gelderblom, A.G. Marin, H. Nair, A. Van Houselt, L. Lefferts, J.H. Snoeijer, D; Lohse, how water droplets evaporate on a superhydrophobic, Phys. Rev. E 83 (2011) 026306.
[48] E. Bormashenko, A. Musin, G. Whyman, M. Zinigrad, wetting Transitions and Depinning of the Triple Line, Langmuir, 28 (2012) 3460−3464.
[49] J.M. Stauber, S.K Wilson, B.R. Duffy, K. Sefiane, on the lifetimes of evaporating droplets, J. Fluid. Mech. 744 (2014) R2.
[50] J.C. Stinville, P. Villechaise, C. Templier, J.P. Rivière, M. Drouet, Lattice rotation induced by plasma nitriding in a 316L polycrystalline stainless steel, Acta Materialia 58 (2010) 2814–2821.
[51] R. Tadmor, line energy and the relation between advancing, receding, and Young contact angles, Langmuir 20 (2004) 7659-7664, (https://doi.org/10.1021/la049410h)
[52] L. Gao, T.J. McCarthy, how Wenzel and Cassie were wrong, Langmuir 23 (2007) 3762-3765, (https://doi.org/10.1021/la062634a).
[53] T. Toth, D. Ferraro, E. Chiarello, M. Pierno, G. Mistura, G. Bissacco, C. Semprebon, suspension of Water Droplets on Individual Pillars, Langmuir 27 (2011), 4742–4748, (https://doi.org/10.1021/la2001249).
[53] B. Zahiri, P. K. Sow, C. H. Kung, W. Mérida, understanding the wettability of rough surfaces using simultaneous optical and electrochemical analysis of sessile droplets, Journal of Colloid and Interface Science 501 (2017) 34–44, (http://dx.doi.org/10.1016/j.jcis.2017.04.043).
[54] D.I. Yu, H.K. Kwak, C. Park, C. Choi, N. P. Sapkal, J. Hong, M.H. Kim, wetting criteria of intrinsic contact angle to distinguish between hydrophilic and hydrophobic micro-/nanotextured urfaces: experimental and theoretical analysis with synchrotron X-ray imaging, Langmuir 35 (2019) 3607−3614, (https://doi.org/10.1021/acs.langmuir.8b03407).
[55] H.C. Kang, A. M. Jacobi, Equilibrium Contact Angles of Liquid Droplets on Ideal Rough Solids, Langmuir 27 (2011) 14910–14918, (https://doi.org/10.1021/la2031413).
[56] C. Semprebon, C. Herrmann, B.Y Liu, R. Seemann, M. Brinkmann, shape evolution of droplets growing on linear microgrooves, Langmuir 34 (2018) 10498−10511, (http://dx.doi.org/10.1021/acs.langmuir.8b01712).

[57] D. Quéré, Wetting and Roughness, Annu. Rev. Mater. Res. 38 (2008) 71–99, (http://dx.doi.org/10.1146/annurev.matsci.38.060407.132434).
[58] J.F. Oliver, C. Huh, S.G. Mason, resistance to spreading of liquids by sharp edges, J. Colloid Interface Sci., 59 (1977) 568−581, (https://doi.org/10.1016/0021-9797(77)90052-2).
[59] Y. Tsoumpas, S. Dehaeck, M. Galvagno, A.Rednikov, H. Ottevaere, U. Thiele, P. Colinet, nonequilibrium Gibbs' criterion for completely wetting volatile liquids, Langmuir, 30 (2014) 11847−11852, (http://dx.doi.org/10.1021/la502708f).
[60] Z. Wang, K. Lin, Y.P. Zhao, the effect of sharp solid edges on the droplet wettability, Journal of Colloid and Interface Science 552 (2019) 563–571, (https://doi.org/10.1016/j.jcis.2019.05.081).
[61] P. Hubbard, D.G. McCulloch, E.D. Doyle, S. J. Dowey, J. N. Georges, a fundamental contribution to a study of the active screen plasma nitriding process. Berg Huettenmaenn Monatsh 151, (2006) 441–445 (https://doi.org/10.1007/BF03165204).
[62] Y. Li, Y. He, S. Zhang, X. He, W. Wang, B. Hu, microstructures and tribological behaviour of oxynitrided austenitic stainless steel, Vacuum, 146, (2017) 1-7, (http://dx.doi.org/10.1016/j.vacuum.2017.09.026).
[63] Y. Li, Y. He, J. Qiu, J. Zhao, Q. Ye, Y. Zhu, J. Mao, enhancement of pitting corrosion resistance of austenitic stainless steel through deposition of amorphous/nanocrystalline oxy-nitrided phases by active screen plasma treatment, Mat. Res. 21 (2018) (http://orcid.org/0000-0002-7680-4959).
[64] T.A.H. Nguyen, A.V. Nguyen, transient volume of evaporating sessile droplets: 2/3, 1/1, or Another Power Law?, Langmuir, **30** (2014) 6544, (https://doi.org/10.1021/la4047287)
[65] D. Hu, H. Wu, volume evolution of small sessile droplets evaporating in stick-slip mode, Phys. Rev. E (2016) **93** 042805 (https://doi.org/10.1103/PhysRevE.93.042805).